JOURNAL OF CATALYSIS 134, 549–571 (1992)

Kinetic Coupling and Hydrogen Surface Fugacities in Heterogeneous Catalysis: I. Alkane Reactions on Te/NaX, H-ZSM5, and Ga/H-ZSM5

ENRIQUE IGLESIA,[1] JOSEPH E. BAUMGARTNER, AND GEOFFREY L. PRICE[2]

Corporate Research Laboratories, Exxon Research and Engineering Company, Route 22 East Annandale, New Jersey 08801

Received March 20, 1991; revised October 2, 1991

Hydrogen removal occurs by recombinative desorption and by hydrogen transfer during dehydrogenation steps required for alkane and cycloalkane conversion on Te/NaX, H-ZSM5, and Ga/H-ZSM5 catalysts. Recombinative desorption limits the rate of *n*-heptane and methylcyclohexane aromatization on Te/NaX and prevents equilibration between gas-phase H_2 and H-adatoms formed in intermediate dehydrogenation steps. The resulting high surface hydrogen fugacities lead to low steady-state concentrations of required unsaturated intermediates. Te ions catalyze rate-limiting hydrogen desorption steps during alkane reactions on Te/NaX. On H-ZSM5, hydrogen removal limits the rate of propane conversion to aromatics. Hydrogen adatoms are removed predominantly by reactions with coadsorbed hydrocarbon fragments, leading to high cracking selectivity. Ga ions introduce a recombinative desorption function that partially relieves the resulting high hydrogen surface fugacities and allows dehydrogenation steps to occur without concurrent cracking. Thus, Ga ions increase aromatics selectivity by providing a "porthole" for the removal of hydrogen adatoms as dihydrogen. We propose that rate-limiting hydrogen desorption steps, and the high surface hydrogen fugacities that result, control the rate and selectivity of dehydrogenation and related reactions on many nonmetal surfaces.

1. INTRODUCTION

Alkane rearrangements proceed via complex reaction sequences on metal and metal oxide surfaces (*1, 2*) and often require dehydrogenated gas-phase and surface intermediates (*3*). Previously, we described the intermediate role of heptenes and *cis*-heptatrienes in *n*-heptane dehydrocyclization on Te/NaX (*4*). Here, we examine the dehydrogenation and hydrogen desorption elementary steps that lead to unsaturated intermediates on Te/NaX, H-ZSM5, and Ga/H-ZSM-5.

Catalytic dehydrogenation, self-hydrogenation, and hydrogen-transfer reactions (*5–7*) involve the release of H-atoms onto surface sites. Here, we show that many of these reactions, specifically alkane dehydrogenation and dehydrocyclization on Te/NaX and on related Ga- and Cr-based materials, are limited by the rate of desorption of these H-adatoms (*4*). Desorption-limited reactions lead to virtual pressures (surface fugacities) that exceed the corresponding gas-phase pressure of the desorbing species (*5, 8*). In effect, the chemical potential of desorbing species increases by kinetic coupling with preceding elementary steps that form them; desorbing species are forced into the gas phase only after a significant increase in their effective surface fugacity and chemical potential.

High hydrogen surface fugacities lead to low steady-state concentrations of alkene, diene, and triene species required in many dehydrocyclization reactions; these con-

[1] To whom correspondence should be addressed.

[2] Permanent address: Department of Chemical Engineering, Louisiana State University, Baton Rouge, LA 70803.

0021-9517/92 $3.00

centrations reflect thermodynamic equilibration with existing surface hydrogen fugacities rather than with gas-phase hydrogen pressures. Our proposed mechanism explains the observed isotopic equilibration of ^{13}C and ^{12}C between alkenes and alkanes, but not between these species and gas-phase deuterium.

We suggest that high hydrogen surface fugacities also occur during hydrogen-transfer (*5, 6*) and disproportionation (*7*) reactions of hydrocarbons on surfaces. They arise because the catalytic surfaces are unable to desorb hydrogen adatoms without raising their chemical potential and fugacity significantly above those in the ambient gas phase. These hydrogen-transfer reactions involve the addition and removal of hydrogen atoms from a surface pool that remains largely nonequilibrated with gas-phase dihydrogen. Consequently, such reactions kinetically resemble bimolecular transfer of H-atoms between two or more adsorbed hydrocarbon species.

2. BACKGROUND

2.1. Catalytic Dehydrogenation/ Dehydrocyclization of Alkanes on Te/NaX Catalysts

Te atoms with X- and Y-zeolites catalyze alkane dehydrocyclization (*9–13*); turnover rates, however, are much lower than on Pt-based catalysts (*4*). Isotopic tracer studies previously suggested that alkenes and other unsaturated species are reactive intermediates in the catalytic sequence (*14–17*). Recent work confirmed these conclusions and provided independent evidence for *n*-heptane dehydrocyclization via thermal electrocyclic addition reactions of *cis*-heptatrienes intermediates (*4*).

2.2 Alkane Dehydrocyclodimerization on H-ZSM5 and Ga/H-ZSM5

Dehydrocyclodimerization of C_2–C_7 alkanes occurs on Pt- (*18–21*) and Ga-(*22–25*) based catalysts by a complex sequence of dehydrogenation, dimerization, and cyclization steps that proceed in parallel with acid-catalyzed and thermal cracking reactions. Ga-based catalysts and moving-bed reactors are used in the CYCLAR process to convert C_2–C_4 alkanes to C_6^+ aromatics (*25*). The oxidation state of Ga during catalysis and its role in the reaction sequence remain unresolved; Ga-catalyzed alkane dehydrogenation (*32*) and alkene cyclization (*24*) have been proposed to explain the enhanced selectivity and activity of Ga-based catalysts in these reactions. Here, we suggest that Ga ions catalyze the desorption of H-adatoms as H_2 and thus lower surface hydrogen fugacities and cracking selectivity.

2.3. Kinetic Coupling and Hydrogen Virtual Pressures at Catalytic Surfaces

Temkin and Pyzhev (*26, 27*) proposed the concept of virtual pressure, created by "pumping" of intermediates onto a surface, to describe the kinetics of ammonia decomposition on Fe. This reaction is limited by recombinative desorption of adsorbed nitrogen atoms (N*), a process that leads to nitrogen virtual pressures (i.e., dinitrogen pressures that would equilibrate with actual steady-state (N*) concentrations) much higher than those in the contacting gas phase. In effect, a virtual equilibrium is defined between any species being interconverted in a rate-limiting (i.e., exergic) step.

Kemball (*5*) used virtual pressure concepts to explain the kinetics of ethane hydrogenolysis and exchange reactions and the selectivity of CH_4/D_2 and CO/H_2 reactions; these reactions lead to surface overpressures of CH_x species. Tamaru and coworkers (*28, 29*) measured nitrogen coverages directly during ammonia decomposition on W and Mo foils by Auger electron spectroscopy. They found that surface nitrogen coverages greatly exceed those present in equilibrium with ambient dinitrogen pressures.

Boudart (*30, 31*) described the kinetic consequences of virtual pressures, more correctly defined as surface fugacities, by applying the De Donder equation for an ele-

mentary step in a catalytic sequence:

$$\frac{\vec{v}_i}{\overleftarrow{v}_i} = e^{A_i/RT}, \tag{1}$$

where A_i is the affinity for the ith reaction step. This reaction affinity is related to the standard reaction affinity

$$A_i^0 = -\Delta G_i^0 \tag{2}$$

by

$$A_i = A_i^0 - RT \ln \prod_i f_i^{\nu_i}, \tag{3}$$

where f_i is the thermodynamic activity or fugacity of species that participate in the ith reaction step as reactants ($\nu_i < 0$) or products ($\nu_i > 0$). An equilibrated elementary step ($A_i = 0$) obeys the usual equilibrium expression

$$\prod_i f_i^{\nu_i} = e^{A_i^0/RT} \tag{4}$$

Rate-limiting steps are exergic ($A_i > 0$) and account for most of the affinity change in the overall reaction. Therefore,

$$\prod_i f_i^{\nu_i} < e^{A_i^0/RT}, \tag{5}$$

and at steady state

$$\frac{\left(\prod_i f_i^{\nu_i}\right)_{ss}}{\left(\prod_i f_i^{\nu_i}\right)_{eq}} < 1. \tag{6a}$$

If subsequent steps are equilibrated, steady-state and equilibrium fugacities of the products of the ith step are equal and Eq. (6a) becomes

$$\frac{\prod_i (f_i^{|\nu_i|})_{eq}}{\prod_i (f_i^{|\nu_i|})_{ss}} < 1, \tag{6b}$$

where f_i refers only to the fugacity of the reactants in the ith step. Clearly, then,

$$\pi_i (f_i^{|\nu_i|})_{ss} > \pi_i (f_i^{|\nu_i|})_{eq}, \tag{6c}$$

and the fugacity of reactants involved in a rate-limiting step must exceed those of the products of the ith step.

Every step in a reaction sequence must occur in the forward direction ($A_i > 0$) for the overall sequence to proceed. Therefore, steps with unfavorable *standard* affinity ($A_i^0 < 0$) must couple kinetically with preceding steps in order to raise the fugacity of reactants to levels required for a positive affinity in the ith step. These conclusions are valid for any nonequilibrated (exergic) step in a steady-state reaction sequence, whether catalytic or not.

3. EXPERIMENTAL METHODS

Catalysts were prepared by ball-milling elemental Te with NaX zeolite (Linde, 13×) for 4 h at room temperature. The initial Te content was 9–10 wt%. The catalyst was activated in flowing dihydrogen at 773 K for 4–6 h before catalytic experiments. Te atoms not stabilized by interactions with cationic sites within zeolite channels sublimed during pretreatment. The Te content in the activated catalyst decreased to 4–5 wt% during the initial pretreatment but remained constant at these levels during subsequent catalytic experiments.

Ga/H-ZSM5 catalysts were prepared by ion exchange of H-ZSM5 (Si/Al = 14.5) with an aqueous solution of Ga nitrate (*32*) at 353 K. The catalyst (2.0 wt% Ga) was pretreated in H_2 at 823 K for 6–8 h before catalytic experiments.

Unlabeled hydrocarbons were obtained from commercial sources [methylcyclohexane (Fluka, 99.6%); *n*-heptane (Fluka puriss grade, >99%); heptenes (Aldrich, Gold Label, >99%); perdeuterated *n*-heptane (MSD Isotopes, >99%, 98.4% D); 3-methyl-1-cyclohexene (Fluka, >99%)]. *n*-Heptane labeled at one terminal carbon position (*n*-[1-^{13}C]heptane) was prepared by catalytic coupling of n-hexyl-magnesium bromide with [^{13}C]methyl iodide (*4*). Hydrogen [Air Products; 99.995%] and deuterium [Air Products; 99.5%] were purified using catalytic (Engelhard, 298 K) and molecular sieve traps (Linde, 13×, 77 K). Propane (Air Products, Research Purity, >99.8%), propene (Air Products, Chemical Purity, >99.2%), and [2-^{13}C]propane (MSD

Isotopes, >99.6% ^{13}C) were obtained from commercial sources and used without further purification.

Catalytic rates and selectivities were measured in a gradientless recirculating batch reactor at reactant conversions less than 25% (*4*). Products were analyzed by capillary column chromatography using flame ionization or electron-impact mass-spectrometric detection. Deuterium distributions in reactants and products were determined using mass spectrometry and a matrix calculation technique reported recently (*33*).

Reaction rates are reported as turnover rates [(moles reactant converted)/(g-atom surface site · s^{-1})]. Selectivity is reported on a carbon–atom basis as the percentage of converted reactant appearing as a given product. The slopes of turnover–time plots give turnover rates for conversion to a given product. Turnovers are defined as the moles of reactant (e.g., *n*-heptane) converted to a given product (e.g., toluene) per gram-atom surface sites in the reactor. Surface sites were assumed to be Te atoms in Te/NaX and Al atoms in H-ZSM5 and Ga/H-ZSM5 in the turnover calculations.

4. *n*-HEPTANE DEHYDROGENATION/ DEHYDROCYCLIZATION ON Te/NaX

Te/NaX catalysts convert *n*-heptane to toluene, isoheptanes, and C_1–C_6 hydrocarbons. Typical product distributions are shown in Table 1. Dehydrocyclization and cracking activation energies are 215 and 230 kJ/mol, respectively. Turnover rates are much lower than on Pt-based catalysts but dehydrocyclization selectivities are similar (*4*).

4.1. Catalytic Turnover Rates and Reaction Pathways

Contact time plots for heptenes suggest that they are reactive intermediates in *n*-heptane dehydrocyclization and isomerization on Te/NaX (Fig. 1). The low initial slopes (turnover rates) and nonzero intercepts of toluene and methylhexane turnover-time plots (Fig. 1) suggest that their formation requires an initial increase in the concentration of a reactive intermediate. *n*-Heptane converts via sequential reactions involving dehydrogenation and cyclization/ isomerization steps. The intermediate role of olefins in dehydrocyclization/isomerization pathways was demonstrated previously using competitive reactions of 1-heptene

TABLE 1

n-Heptane Conversion Rates and Selectivity on Te/NaX (97 kPa H_2, 4.4 kPa C_7H_{16})

Temperature (K)	723	773
n-Heptane conversion (%)	9.8	23.5
Turnover Rate (v/s^{-1})	4.0×10^{-4}	3.5×10^{-3}
Carbon selectivity (%)		
C_1	0.9	2.4
C_2	1.9	4.1
C_3	3.6	6.2
C_4	8.3	8.9
C_5	3.1	6.9
C_6 (aliphatic)	0.9	1.2
Benzene	2.6	5.6
Dimethylpentanes	0.1	0.1
2-Methylhexane	5.8	1.4
3-Methylhexane	7.4	1.5
Ethylpentane	0.9	0.3
Ethylcyclopentane	0.8	0.5
Dimethylcyclopentanes	0.1	0.1
Toluene	34.6	38.0
Heptenes	Balance	Balance
Cracking/aromatization ratio	0.50	0.68

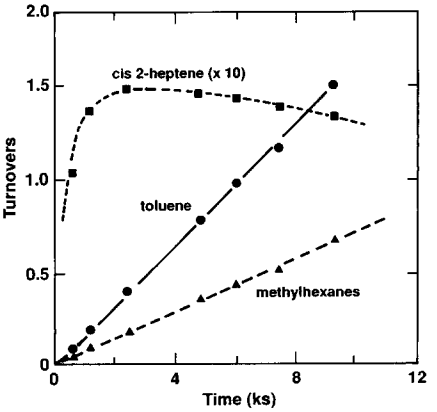

FIG. 1. *n*-Heptane reactions on Te/NaX. Toluene, methylhexanes, and *cis*-2-heptene turnovers (*n*-heptane, 4.6 kPa; dihydrogen, 96 kPa; 723 K; maximum heptane conversion 25%).

and *n*-[1-^{13}C]heptane (*4*). Subsequent olefin dehydrogenation steps give heptatriene intermediates that undergo thermal cyclization, consistent with the isotopomer distribution in toluene formed from *n*-[1-^{13}C] heptane reactants and with the low cyclization rate of molecules that are unable to form triene species (e.g., 3,3-dimethylhexane) (*4*).

4.2. *Catalytic Dehydrocylization Sequence*

Heptene turnovers (Fig. 1) and heptene/*n*-heptane ratios (Fig. 2) reach constant values after about 2 ks, suggesting a steady-state reaction scheme that involves sequential dehydrogenation steps (*13*):

$$C_7H_{16} \underset{k_{-1}}{\overset{k_1}{\rightleftharpoons}} C_7H_{14} + H_2 \quad (7a)$$

(*n*-heptane) (*n*-heptenes)

$$C_7H_{14} \underset{k_{-2}}{\overset{k_2}{\rightleftharpoons}} C_7H_{12} + H_2 \quad (7b)$$

(*n*-heptenes) (*n*-heptadienes)

$$C_7H_{12} \underset{k_{-3}}{\overset{k_3}{\rightleftharpoons}} C_7H_{10} + H_2 \quad (7c)$$

(*n*-heptadienes) (*n*-heptatrienes)

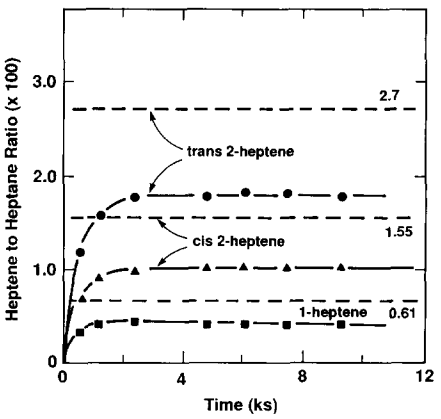

FIG. 2. Heptene to *n*-heptane ratios (*n*-heptane, 4.6 kPa; dihydrogen, 96 kPa; 723 K; maximum heptane conversion 25%).

$$C_7H_{10} \underset{k_{-4}}{\overset{k_4}{\rightleftharpoons}} C_7H_{10} \quad (7d)$$

(*cis*-heptatriene) (methylcyclohexadienes)

$$C_7H_{10} \underset{k_{-5}}{\overset{k_5}{\rightleftharpoons}} C_7H_8 + H_2 \quad (7e)$$

(methylcyclohexadienes) (toluene)

Each dehydrogenation step also involves a sequence of reversible elementary steps that include hydrocarbon adsorption (8a), sequential H-atom abstraction (8b, 8c), and desorption of hydrocarbon (8d) *and* hydrogen (8f) products:

$$C_7H_{16} + * \rightleftarrows C_7H_{16}* \quad (8a)$$

$$C_7H_{16}* + * \rightleftarrows C_7H_{15}* + H* \quad (8b)$$

$$C_7H_{15}* + * \rightleftarrows C_7H_{14}* + H* \quad (8c)$$

$$C_7H_{14}* \rightleftarrows C_7H_{14} + * \quad (8d)$$

$$C_7H_{16} + 2* \underset{k_{-1}}{\overset{k_1'}{\rightleftarrows}} C_7H_{14} + 2H* \quad (8e)$$

$$H* + H* \underset{k_a}{\overset{k_d}{\rightleftarrows}} H_2 + 2*. \quad (8f)$$

At steady state, the alkene/alkane ratio in the overall reaction scheme (Eq. (7)) reaches a constant value given by

$$R_{ss} = \frac{(C_7H_{14})}{(C_7H_{16})} = k_1 \Big/ \left(k_2 + k_{-1} - \left[\frac{k_{-2}k_2(k_4 + k_{-3})}{(k_3k_4 + k_{-2}k_4 + k_{-2}k_{-3})}\right]\right), \quad (9)$$

where the pseudo-first-order rate constants include any kinetic dependence on surface hydrogen (H*). When every step in Eq. (8) is equilibrated ($k_{-i} \gg k_{i+1}$), heptene to heptane ratios become

$$R_{eq} = \left(\frac{C_7H_{14}}{C_7H_{16}}\right) = \frac{k_1}{k_{-1}(H_2)_g} = \frac{\overline{K}_1}{(H_2)_g} \quad (10)$$

If steps in Eq. (8) except for H* desorption are equilibrated, the equilibrium expression for Eq. (8e)

$$\frac{k_1'}{k_{-1}'} = \frac{(C_7H_{14})(H^*)_{ss}^2}{(C_7H_{16})(^*)_{ss}^2} \tag{11a}$$

gives a steady-state alkene to alkane ratio

$$R_{ss} = \frac{k_1'}{k_{-1}'}\frac{(^*)_{ss}^2}{(H^*)_{ss}^2}. \tag{11b}$$

The surface hydrogen fugacity $(H_2)_{ss}$ is defined as the equivalent hydrogen pressure that would be in equilibrium with $(H^*)_{ss}$; it is given by

$$(H_2)_{ss} = \frac{k_d}{k_a}\cdot\frac{(H^*)_{ss}^2}{(^*)_{ss}^2}. \tag{11c}$$

Equation (11b) then becomes

$$R_{ss} = \frac{k_1'}{k_{-1}'}\frac{k_d}{k_a}\cdot\frac{1}{(H_2)_{ss}} = \frac{\bar{K}_1}{(H_2)_{ss}} \tag{11d}$$

$$= R_{eq}\left[\frac{(H_2)_g}{(H_2)_{ss}}\right],$$

where $(H_2)_g$ is the ambient gas phase dihydrogen pressure. This expression reduces to its true equilibrium value when hydrogen adsorption–desorption steps are also equilibrated:

$$(H_2)_{ss} = (H_2)_g \tag{11e}$$

$$R_{ss} = R_{eq} = \frac{\bar{K}_1}{(H_2)_g}. \tag{11f}$$

If the *n*-heptane dehydrogenation step at steady state is far from equilibrium (i.e., $k_{i+1} \gg k_{-i}$, exergic), alkene/alkane ratios are given by

$$\frac{(C_7H_{14})}{(C_7H_{16})} = \frac{k_1}{k_2}. \tag{12}$$

Its value depends on the kinetics of dehydrogenation of alkanes (k_1) and alkenes (k_2).

The ratio of the observed [(R_{ss})], to the equilibrated [R_{eq}, Eq. (11f)] heptene/heptane ratio is obtained by a similar procedure using a more general form of Eq. (9) and given by

$$\chi = \frac{R_{ss}}{R_{eq}} = \frac{(H_2)_g/(H_2)_{ss}}{\left(1 + \frac{k_2}{k_{-1}}\right)}, \tag{13}$$

irrespective of whether dehydrogenation or subsequent reactions of olefin intermediates limit the overall rate. This expression suggests two potential mechanisms for deviations of heptene/heptane ratios from equilibrium values: a high hydrogen surface fugacity [$(H_2)_{ss} > (H_2)_g$] or an incomplete equilibration of the heptane dehydrogenation step ($k_{-1} < k_2$).

Figure 2 describes experimental heptene/heptane ratios for 1-, *cis*-2-, and *trans*-2-heptenes; they approach a constant value after about 2 ks for all heptene isomers. The dashed lines show the equilibrium value expected for each alkene isomer at reaction temperature and gas-phase dihydrogen pressure (96 kPa) (*4*, *34*). Experimental and equilibrium heptene/heptane ratios differ significantly. The observed constant values of heptene/heptane ratio, therefore, appear to reflect nonequilibrated heptene concentrations. The ratio of experimental (steady state) to equilibrium alkene to alkane ratios (χ, Eq. (13)) is less than one and very similar for all heptenes (1-heptene, 0.66; *cis*-2-heptene, 0.64; *trans*-2-heptene 0.66, at 96-kPa dihydrogen pressure; Table 2). These data suggest that in the absence of hydrogen surface overpressures [$(H_2)_g/(H_2)_{ss} = 1$], the kinetic constant ratio (k_2/k_{-1}) would be 0.5–0.6 and independent of the double-bond

TABLE 2

Equilibrium and Steady-State Heptene to Heptane Ratios on Te/NaX (723 K, 4.4 kPa *n*-Heptane)

Dihydrogen pressure (kPa)	(Heptene/heptane) Ratio × 10^2		
	1-Heptene	*cis*-2-Heptene	*trans*-2-Heptene
	(a) Equilibrium		
20	2.96	7.60	13.2
47	1.48	3.26	5.65
96	0.61	1.56	2.71
	(b) Steady-State		
20	0.58	1.32	2.35
47	0.51	1.2	2.15
96	0.40	1.0	1.8
	(c) Ratio of steady-state to equilibrium values		
20	0.194	0.175	0.178
47	0.347	0.367	0.380
96	0.66	0.64	0.66

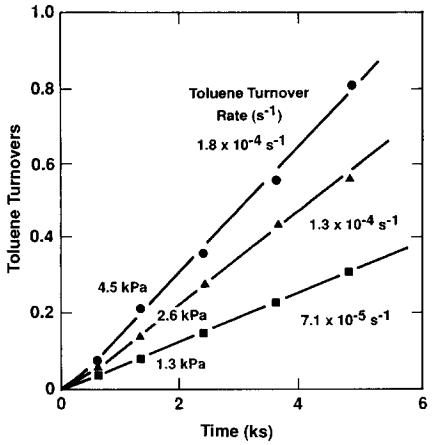

FIG. 3. *n*-Heptane pressure effects on toluene turnovers (*n*-heptane, 1.3-4.6 Pa; dihydrogen, 96 kPa; 723 K).

position in alkenes. Such rate constant ratios, however, are much lower than those obtained from reactions of *n*-[1-^{13}C]heptane/1-heptene mixtures and reported below, suggesting that surface hydrogen fugacities exceed the gas-phase dihydrogen pressure.

4.3. *n*-Heptane

Dehydrocyclization Kinetcs

Steady-state dehydrocyclization turnover rates and heptene concentrations are proportional to *n*-heptane pressure (Fig. 3), consistent with previously reported kinetics (*13*). Toluene turnover plots show nonzero intercepts, suggesting that initial turnover rates are zero at all heptane pressures (Fig. 3). Turnover rates increase as contact time increases; they reach steady-state values (reported in Fig. 3) after about 1–2 ks, the contact times required to achieve steady-state concentrations of heptene intermediates.

Steady-state dehydrocyclization turnover rates are inversely proportional to dihydrogen pressure between 20 and 96 kPa (Fig. 4a). Asymptotic alkene/alkane ratios increase only slightly as dihydrogen pressure decreases (Fig. 4b); they do not obey the inverse dependence expected for equilibrated dehydrogenation steps. Steady-state and equilibrium ratios for terminal and internal heptene intermediates are shown in Table 2 at several dihydrogen pressures. Deviations from equilibrium (χ) increase as dihydrogen pressure decreases; they are similar for all heptene isomers. These data suggest that the initial dehydrogenation step is nonequilibrated; the reaction sequence essentially consists of rate-determining sequential dehydrogenation steps. Alternately, these data could reflect a surface hydrogen pool that remains nonequilibrated with gas-phase dihydrogen.

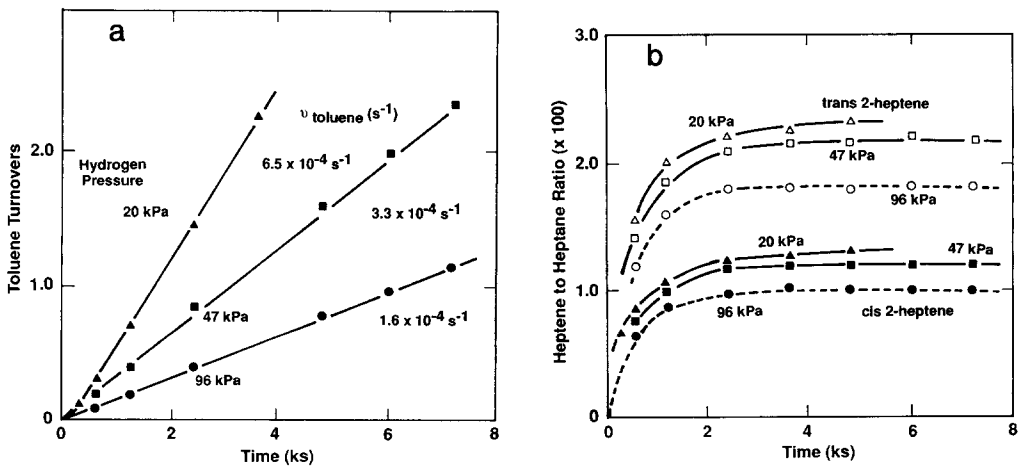

FIG 4. Dihydrogen pressure effects on *n*-heptane reactions. (a) Toluene turnovers. (b) Heptene to heptane ratios (*n*-heptane, 4.6 kPa; dihydrogen, 96 kPa; 723 K).

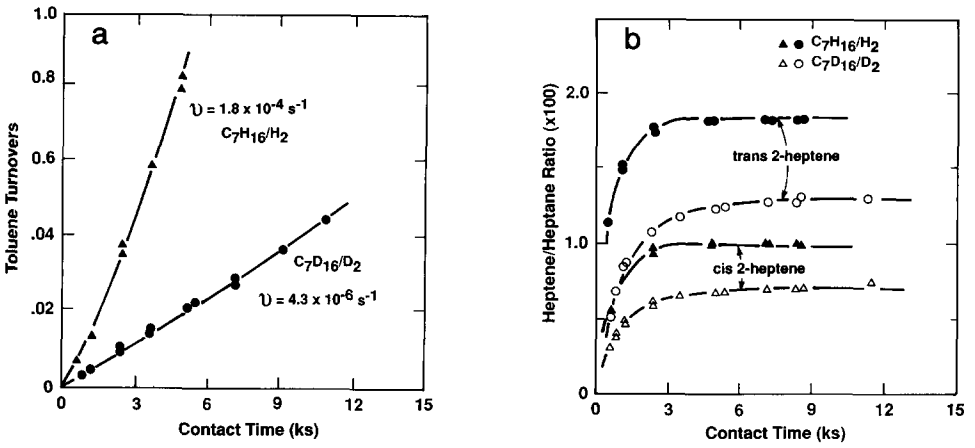

FIG. 5. Kinetic isotope effects (C_7H_{16}/H_2 vs C_7D_{16}/D_2). (a) Toluene turnovers. (b) Heptene to heptane ratios (*n*-heptane, 4.6 kPa; dihydrogen, 20–96 kPa; 723 K).

4.4. Dehydrocyclization Kinetic Isotope Effects in n-Heptane

Dehydrocyclization and dehydrogenation turnovers for *n*-heptane (C_7H_{16} in H_2) and perdeuterated *n*-heptane (C_7D_{16} in D_2) reactants are compared in Fig. 5. A large kinetic isotope effect is observed; toluene turnover rates are 4.3 times lower (Fig. 5a) and asymptotic heptene/heptane ratios (Fig. 5b) are 1.5 times lower for perdeuterated reactants. The observed dehydrocyclization kinetic isotope effects are greater than those expected from a single rate-determining dehydrogenation step in an irreversible sequence; thus, it is inconsistent with a totally irreversible reaction sequence, whose overall rate equals the unidirectional forward rate of the initial dehydrogenation step. The kinetic isotope effect for the initial (irreversible) *n*-heptane dehydrogenation to heptenes on Te/NaX is about 2.0, considerably lower than the value of 4.3 obtained for the overall catalytic sequence. The observed effect of deuterium substitution on heptene/heptane ratios (KIE = 1.5) is somewhat weaker than that for *n*-heptane reactions on Pt catalysts (1.7–1.9) (*35*); the latter reflects isotopic effects on the hydrogenation–dehydrogenation equilibrium constant. Isotope effects on heptene/heptane ratios on Te/NaX (~1.5) are unlikely to reflect only deuterium effects on (k_2/k_1) ratios, which determine heptene/heptane ratios for an irreversible sequence (Eq. (12)). Such isotope effects should approach unity because of the similar expected kinetic isotope effects in the consecutive alkane and alkene dehydrogenation steps.

Kinetic isotope effects on Te/NaX (4.3) are consistent with a sequence of surface-catalyzed dehydrogenation steps (7a)–(7c), (7e) where alkane/alkene adsorption, desorption, and interconversion are in quasi-equilibrium but where the overall reaction rate is limited by the hydrogen-desorption step that accompanies each dehydrogenation event; it must occur four times for the formation of a toluene molecule. The overall rate of such a reaction sequence is given by

$$\upsilon = \frac{\overline{\mathbf{K}}_4\overline{\mathbf{K}}_5\,\overline{\mathbf{K}}_1\overline{\mathbf{K}}_2\overline{\mathbf{K}}_3\,(C_7H_{16})}{(H_2)_{ss}^4} \qquad (14)$$

If deuterium isotope effects measured for heptane dehydrogenation on Te/NaX (*35*) (~1.5) apply for subsequent dehydrogenation steps, and if the equilibrium constant for the thermal electrocyclic addition reaction of heptatrienes is unaffected by deuterium substitution because it involves concerted C–H bond-breaking and bond-

making steps, the calculated kinetic isotope effect for the overall sequence is 5.0, in qualitative agreement with the observed value of 4.3.

The rate-limiting recombinative desorption of deuterium leads to large kinetic isotope effects because of the higher binding energy of deuterium atoms on most surfaces and because deuterium desorption must occur four times in one dehydrocyclization turnover.

4.5 Isotopic Tracer Studies of 1-Heptene Reaction Pathways

The intermediate role of heptenes and their relative rates of hydrogenation (to heptane) and conversion to products were established by measuring the rate of appearance of unlabeled heptane and of unlabeled toluene, isoheptanes, and C_1–C_6 products from 1-heptene (~25% mol) and *n*-[1-^{13}C]heptane (~75% mol) reactant mixtures.

Figure 6 shows the ^{13}C content in *n*-heptane, heptenes, and toluene at dihydrogen pressures of 20 kPa (Fig. 6a) and 96 kPa (Fig. 6b). The ^{13}C content in all heptenes is similar, suggesting that ^{13}C equilibration occurs rapidly among heptene isomers. Isotopic equilibration between heptenes and *n*-heptane proceeds more slowly; isotopic contents become equal at contact times greater than about 2 ks, suggesting that isotopic, and therefore chemical, equilibration eventually occurs between heptane and heptenes. Toluene is preferentially formed from unlabeled heptenes, suggesting that alkene intermediates are required in dehydrocyclization reactions. The intermediate role of unsaturated species in dehydrocyclization is consistent with alkane cyclization via thermal electrocyclic addition reactions of heptatriene intermediates (*4*). Initial methylhexane and C_1–C_6 products are also unlabeled, suggesting that heptenes are also required intermediates in isomerization and cracking reactions.

These results suggest that ^{13}C isotopic equilibration occurs between *n*-heptane and 1-heptene at contact times similar to those required for attaining steady-state heptene/heptane ratios. Yet, these ratios are well below equilibrium values. ^{13}C equilibration between *n*-heptane and heptenes occurs rapidly; yet, it must occur

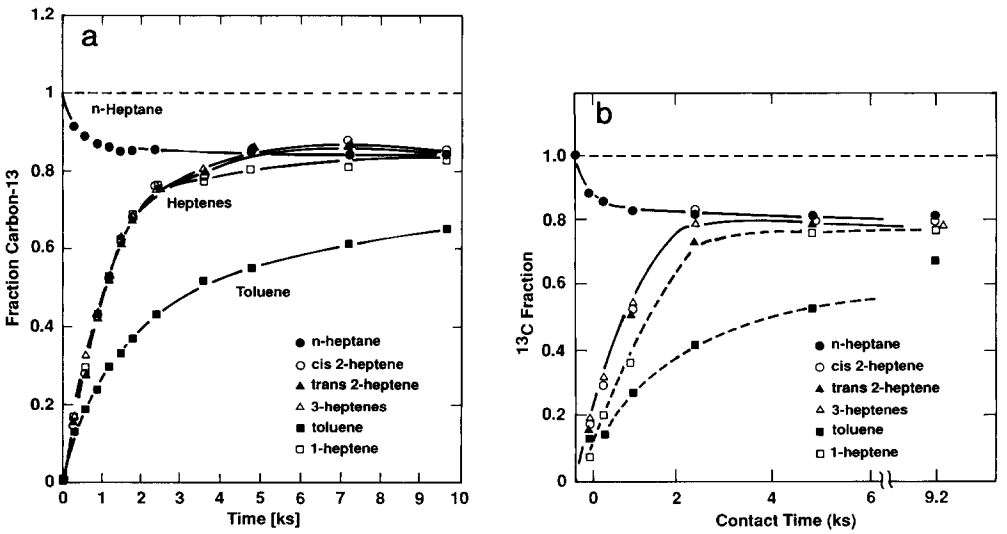

FIG. 6. Competitive reactions of *n*-[1-^{13}C]heptane/1-heptene mixtures. Isotopic composition of *n*-heptane, heptenes, and toluene. (a) 20-kPa dihydrogen pressure. (b) 96-kPa dihydrogen pressure (*n*-[1-^{13}C]Heptane, 3.3 kPa; unlabeled 1-heptene, 1.1 kPa; 723 k).

on a surface where steady-state hydrogen fugacities significantly exceed ambient gas-phase pressures. Thus, the overall dehydrogenation rate is not limited by C–H bond-breaking steps in *n*-heptane or heptene surface reactions (8a)–(8d), but by the recombinative desorption of the resulting hydrogen adatoms (8f).

Unlabeled *n*-heptane (v_H) and product formation (v_T) turnover rates from 1-heptene/*n*[1-^{13}C]heptane reactants (Fig. 7) reflect the net rates of heptene hydrogenation and of all other heptene conversion reactions at steady state:

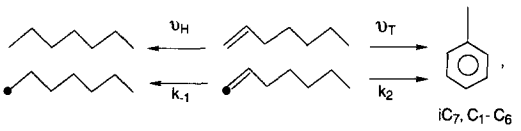

(15)

The unidirectional (initial) reaction rates during the tracer study are given by

$$v_H = k_{-1}(C_7H_{14}) \quad (16)$$
$$v_T = k_2(C_7H_{14}).$$

The measurement of undirectional rates requires that unlabeled olefin and labeled *n*-heptane pools remain largely uncontaminated by isotopic scrambling; therefore, rates are obtained by extrapolating the data in Fig. 7 to zero-contact time.

TABLE 3

Relative (Initial) Rates of Olefin Hydrogenation (v_H) and Olefin Dehydrocyclization/Isomerization (v_T) Obtained from ^{13}C and Deuterium Exchange Rates

	From ^{13}C exchange	From deuterium exchange
(a) 20-kPa dihydrogen (dideuterium) pressure		
v_H (s^{-1})	5.6×10^{-3}	8.0×10^{-4}
v_T (s^{-1})	1.0×10^{-3}	7.2×10^{-4}
v_T/v_H	0.18	0.90
(b) 96-kPa dihydrogen (dideuterium) pressure		
v_H (s^{-1})	7.3×10^{-3}	1.7×10^{-3}
v_T (s^{-1})	6.5×10^{-4}	4.5×10^{-4}
v_T/v_H	0.09	0.26

Extrapolated rates obtained from turnovers vs contact-time plots of [^{12}C]toluene (and all other products requiring [^{12}C]heptene) (Fig. 7) are reported in Table 3. The ratio of ^{12}C product turnovers (toluene and other products) to *n*-[^{12}C]heptane turnovers, extrapolated to zero chemical and isotopic

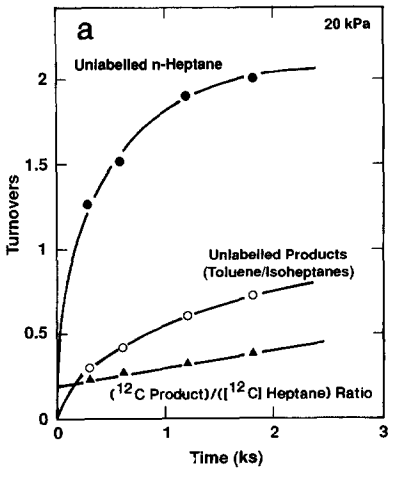

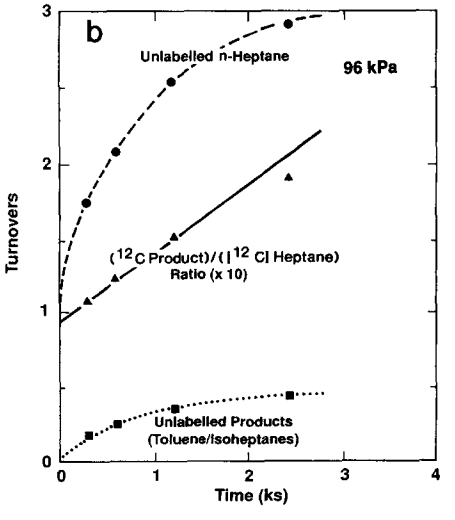

FIG. 7. Competitive reactions of *n*-[1-^{13}C]heptane/1-heptene mixtures. Turnover rates for formation of unlabeled products and *n*-heptane. (a) 20-kPa hydrogen pressure. (b) 96-kPa hydrogen pressure (*n*-[1-^{13}C]Heptane, 3.3 kPa; unlabeled 1-heptene, 1.1 kPa; 723 K).

conversion, gives a direct measurement of (k_2/k_{-1}):

$$\frac{v_T}{v_H} = \frac{k_2}{k_{-1}}; \qquad (17)$$

experimental results provide only an upper limit for this ratio because rapid isotopic equilibration prevents direct measurements at low isotopic conversion, and the effect of reverse reactions (*n*-heptane dehydrogenation) is to decrease the net rate of ^{12}C appearance in *n*-heptane. These ratios of rate constants (Eq. (8)) are 0.18 and 0.09 at 20- and 96-kPa dihydrogen pressures, respectively (Table 3). These values are upper limits; yet, they are considerably smaller than those calculated from deviations of steady-state alkene/alkane ratios from their equilibrium values (Table 2).

These (k_2/k_{-1}) ratios measured from isotopic exchange rates are small; they suggest that dehydrogenation–hydrogenation steps involving carbon atoms are quasi-equilibrated during steady-state dehydrocyclization of *n*-heptane. For example, the expected 1-heptene/*n*-heptane ratios (in the case of equilibrated hydrogen adsorption–desorption) for these values of (k_2/k_{-1}) are 0.55×10^{-2} and 2.51×10^{-2} at 96- and 20-kPa dihydrogen pressures, respectively; the corresponding experimental values are significantly lower (0.40×10^{-2} and 0.58×10^{-2}), especially at low dihydrogen pressures. The marked differences between steady-state and equilibrium heptene/heptane ratios, their weak dependence on dihydrogen pressure and the low (k_2/k_{-1}) values reported in this section suggest that isotopic carbon equilibration occurs rapidly during *n*-heptane reactions on Te/NaX but *without concurrent equilibration between gas-phase and surface hydrogen species*. In other words, desorption of hydrogen from the surface is a rate-determining (exergic) step that prevents complete equilibration between H_2 and hydrogen adatoms produced in sequential dehydrogenation steps.

In effect, dehydrogenation elementary steps (8a)–(8d) divert some of the overall affinity change of the dehydrogenation sequence into raising the chemical potential (fugacity) of hydrogen adatoms in order to overcome an unfavorable standard affinity (A_i^0) in the hydrogen desorption step (8f). As a result, the rate of *n*-heptane dehydrogenation decreases. Hydrogen desorption limitations lead to high hydrogen surface fugacities; dehydrocyclization rates decrease because the concentration of unsaturated reaction intermediates are limited to values in equilibrium with a high surface hydrogen fugacity rather than with the lower gas-phase dihydrogen pressure.

4.6.n-Heptane–Deuterium Exchange

The rate of isotopic exchange between gas-phase deuterium and *n*-heptane provides an independent value of the ratio of alkene hydrogenation (v_H) to net alkene dehydrocyclization, isomerization, and cracking (v_T). In effect, these data can show whether surface hydrogenation reactions use H-atoms cleaved from *n*-heptane reactants or D-adatoms equilibrated with gas-phase D_2. The distribution of deuterium in unreacted *n*-heptane and in *cis*-2-heptene and toluene products of *n*-heptane/D_2 mixtures are shown in Fig. 8 at several contact times and 20- and 96-kPa D_2. At short contact times, the gas phase, and any adsorbed species in equilibrium with it, contain no protium species. *n*-Heptane-d_1 and -d_2 species are the most abundant deuterated species at short contact times; they reflect the weak contribution of gas-phase deuterium to the surface hydrogen pool and to the hydrogenation (v_H) of olefin intermediates.

More highly deuterated *n*-heptane, with a binomial deuterium distribution centered at about d_5–d_6, is formed by hydrogenation of intermediate olefins that previously underwent secondary deuterium–exchange reactions; these reactions occur rapidly on cationic sites within NaX zeolites during double-bond isomerization of intermediate olefins (*36*). They result in toluene and olefin deuterium contents significantly higher than

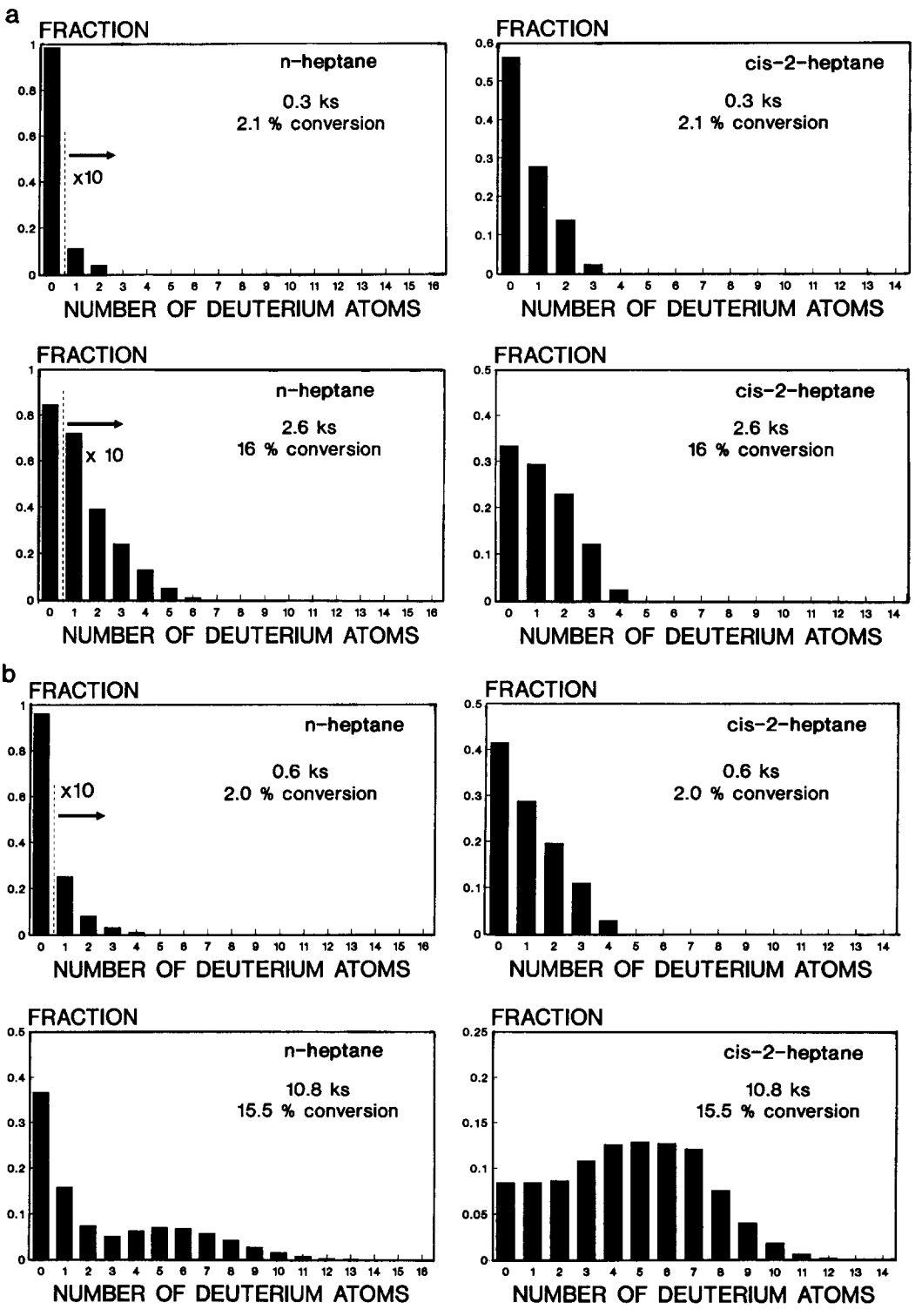

FIG. 8. *n*-Heptane/deuterium reactions. Deuterium distribution in *n*-heptane and *cis*-2-heptene. (a) 20-kPa dideuterium pressure. (b) 96-kPa dideuterium pressure (*n*-heptane, 4.5 kPa; 723 K).

those in unreacted *n*-heptane. The similar binomial shape of the d_3–d_{14} deuterium distributions in heptenes and heptanes suggest that deuteration or hydrogenation of extensively exchanged heptenes accounts for multiply-exchanged *n*-heptane. The marked differences in d_0–d_2 distribution and in total deuterium content between heptane and heptenes, however, demonstrate the lack of H–D isotopic exchange between heptenes and heptane in contact times that suffice for ^{13}C isotopic equilibration. The low deuterium content (<3% D) in "unreacted" *n*-heptane at these short contact times (~2 ks) suggests that heptene hydrogenation steps use predominantly protium (from *n*-heptane) rather than deuterium adatoms (from gas-phase D_2).

The presence of deuterium atoms in *n*-heptane reactants suggests a partially reversible dehydrogenation–hydrogenation sequence:

$$C_7H_{16} + * \rightleftarrows C_7H_{16^*} \quad (18a)$$

$$C_7H^*_{16} + * \rightleftarrows C_7H_{15^*} + H(D)^* \quad (18b)$$

$$C_7H^*_{15} + * \rightleftarrows C_7H_{14^*} + H(D)^* \quad (18c)$$

$$C_7H^*_{14} \rightleftarrows C_7H_{14} + * \quad (18d)$$

$$H(D)^* + H(D)^* \rightleftarrows H_2\,(D_2). \quad (18e)$$

Steady-state *n*-heptane turnover rates are given by the rate of appearance of toluene and methylhexane products (cracking selectivities are less than 15%) that require olefin intermediates (*4*). The ratio of the rate of deuterium incorporation into heptane (the exchange rate, v_D), which occurs during reversible dehydrogenation–hydrogenation steps, to the heptane conversion rate gives the fraction of the reactive surface hydrogen pool that consists of deuterium (from D_2). Thus, we obtain a direct measurement of the hydrogen surface fugacity. These calculations assume that H–D kinetic isotope effects in C_7H_{16}/D_2 mixtures are small; experimental isotope effects for dehydrogenation of C_7H_{16}/D_2 mixtures are less than 1.2.

Deuterium incorporation into *n*-heptane occurs in at least two ways: (a) by a reversible dehydrogenation–hydrogenation reaction event without intermediate deuterium exchange into reactive heptenes (leading to *n*-heptane-d_2 if the surface is equilibrated with gas-phase D_2), or (b) by a similar reversible step, but after fast exchange of intermediate heptenes with deuterium (leading to *n*-heptane-(d_3–d_{16})). *n*-Heptane-d_1 products must arise from similar pathways on a surface containing both H- and D-atoms or from an incomplete traversal of the reversible dehydrogenation–hydrogenation step (Eq. (19)). Thus, we calculate turnover rates for exchange (i.e., hydrogenation using the gas-phase source of hydrogen) from the rate of formation of *n*-heptane molecules containing one or more deuterium atoms. Deuterated *n*-heptane turnovers (Fig. 9) are calculated from the number of d_1 (multiplied by 0.5 to account for its acquiring only one deuterium in the hydrogenation step) and d_{2+} *n*-heptane molecules in the product.

We consider every *n*-heptane molecule containing one or more deuterium atoms to have made one reactive sojourn on a surface containing only D* and thus instantaneously and completely equilibrated with gas-phase D_2. The rate of heptane deuteration is then given by the slope of the deuteration turnover-contact time plots shown in Fig. 9. The steady-state conversion rate of heptenes to products (v_T) is given by the accompanying total turnover-contact time plot (Fig. 9).

The (v_T/v_D) ratios obtained from deuterium exchange data are considerably larger than (v_T/v_H) ratios obtained from ^{13}C isotopic tracer studies (e.g., 0.90 vs 0.18 at 20 kPa; 0.26 vs 0.09 at 96 kPa gas-phase pressures) (Table 4). The ^{13}C tracer experiments give a kinetic ratio for a hydrogenation event

$$\left(\frac{v_H}{v_T}\right) = \left(\frac{k_{-1}}{k_2}\right)\Bigg|^{13}C = \frac{k'_{-1} \cdot (H^*)_{Total}}{k_2} \quad (19)$$

that reacts with the entire hydrogen surface pool, whether equilibrated with gas-phase hydrogen species or not. Deuterium exchange rates, however, measure only those

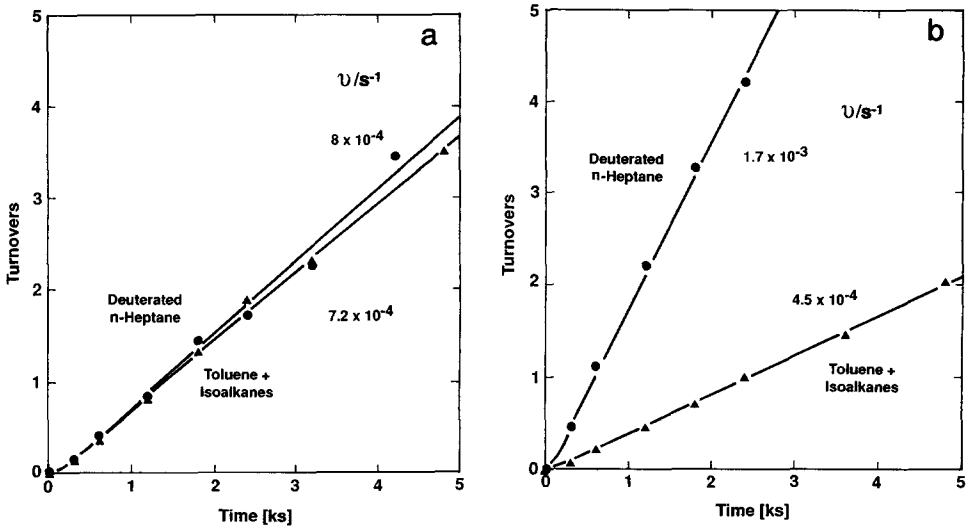

FIG. 9. Turnover rates for deuterated *n*-heptane and product formation from *n*-heptane/D_2 mixtures. (a) 20-kPa deuterium pressure. (b) 96-kPa deuterium pressure (*n*-heptane, 4.5 kPa; 723 K; deuterated heptane turnovers calculated from concentration of d_{2+} species plus 0.5 times the concentration of d_1 species).

hydrogenation (deuteration) steps that use sites equilibrated with the (predominantly) deuterium gas phase,

$$\left(\frac{\upsilon_D}{\upsilon_T}\right) = \left(\frac{k_{-1}}{k_2}\right)\Bigg|_D = \frac{k'_{-1}\cdot(D^*)}{k_2}. \quad (20)$$

TABLE 4

Kinetic Rates and Hydrogen Surface Fugacities during *n*-Heptane Dehydrocyclization on Te/NaX (723 K, 4.4 kPa, *n*-Heptane)

Gas-phase $H_2(D_2)$ pressure (kPa):	96	20
(υ_H/υ_T) from ^{13}C exchange	11.1	5.5
(υ_H/υ_T) from deuterium exchange	3.85	1.1
(υ_H/υ_T) from heptene/heptane ratio[a]	1.86	0.21
$(H_2)_{ss}/(H_2)_g$[b]	1.40	4.8
$(H_2)_{ss}$/kPa	135	96
% Deuterium in surface pool[c]	34	20
% Deuterium in toluene product[d]	33	18

[a] From Eq. (14) assuming $(H_2)_{ss}/(H_2)_g = 1.0$.
[b] From Eq. (14) and ^{13}C exchange kinetics.
[c] From ratio of (k_{-1}/k_2) from deuterium exchange to that from ^{13}C tracers.
[d] At ~5% conversion of *n*-heptane.

Thus, the ratio

$$\left(\frac{\upsilon_D}{\upsilon_H}\right) = \frac{(k_{-1}/k_2)_D}{(k_{-1}/k_2)^{13}C} = \frac{(D^*)}{(H^*)_{Total}} \quad (21)$$

provides an estimate of the fraction of the surface pool that consists of D* and is therefore equilibrated with gas-phase deuterium. These fractions are 0.20 and 0.34 at 20 and 96 kPa deuterium, respectively (Table 4). These values agree well with the observed fraction of deuterium in toluene (0.18 and 0.33); toluene molecules exchange rapidly with surface hydrogen species and thus sample the composition of the hydrogen surface pool on Te/NaX (Table 4).

These data show that the hydrogen surface fugacity is 1.4 times greater than gas-phase pressures at 96 kPa and 4.8 times greater at 20 kPa during *n*-heptane reactions on Te/NaX (Table 4). Surface fugacity values determine surface reaction rates; the kinetic behavior of this surface is identical to that observed on surfaces actually *equilibrated* with similar gas-phase dihydrogen fugacities.

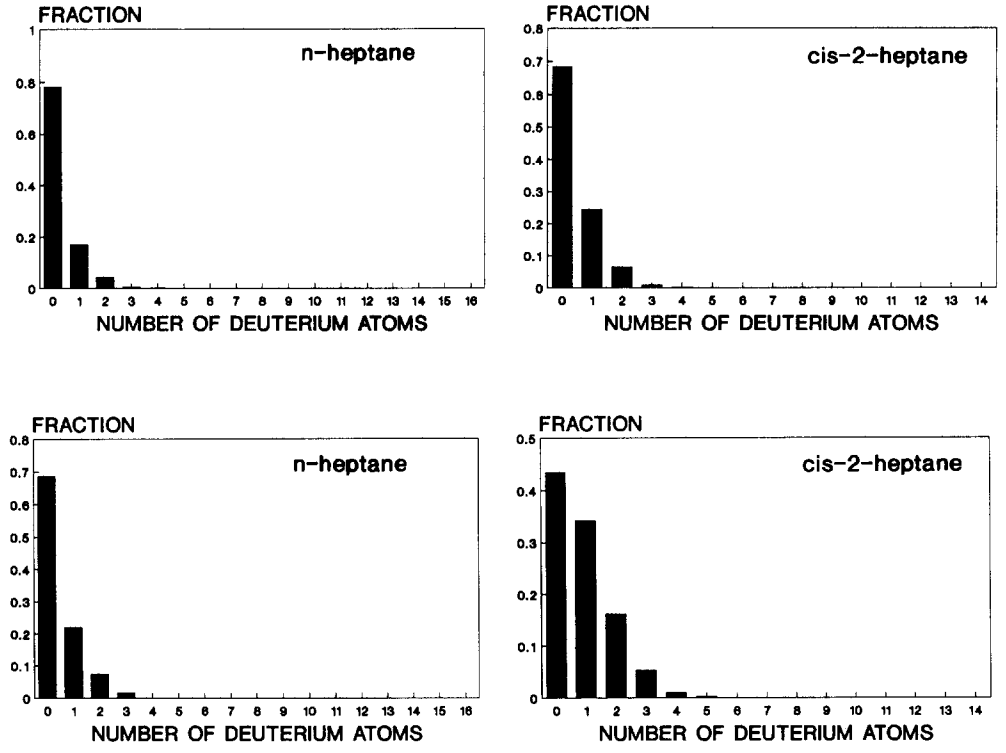

FIG. 10. Deuteration of 1-heptene on Te/NaX. Initial deuterium distributions in *n*-heptane and *cis*-2-heptene (1-heptene, 1.3 kPa; deuterium, 20 kPa; 723 K; top, 0.3 ks, 88.2% conversion; bottom, 0.6 ks, 93% conversion).

4.7.1-Heptene Deuteration Rates

The initial deuterium content in *n*-heptane formed during dehydrocyclization of C_7H_{14}/D_2 (Fig. 10) or $C_7H_{14}/C_7D_{16}/D_2$ mixtures (Fig. 11) is very low, also suggesting that high hydrogen surface fugacities exist during alkene dehydrogenation reactions on Te/NaX. 1-Heptene undergoes dehydrogenation and dehydrocyclization reactions that release hydrogen (H*) onto the surface and hydrogenation, which consumes H* and any D* equilibrated with D_2. 1-Heptene reacts much more rapidly than *n*-heptane; therefore, surface hydrogen fugacities arise mostly from C_7H_{14} dehydrogenation rather than from C_7D_{16} reactions in $C_7H_{14}/C_7D_{16}/D_2$ mixtures. *n*-Heptane-d_2 is the expected initial product of 1-heptene hydrogenation if only D* is present at the surface (i.e., equilibrated hydrogen adsorption–desorption); *n*-heptane-d_0 forms only if surface hydrogen fugacities significantly exceed gas-phase D_2 pressures.

The most abundant initial product of 1-heptene reactions in D_2 (Fig. 10) or C_7D_{16}/D_2 (Fig. 11) mixtures on Te/NaX catalysts pretreated with H_2 (but subsequently exchanged with D_2 at reaction conditions for 0.6 ks before reaction) is *n*-heptane-d_0. The initial *n*-heptane product (0.3 ks, Fig. 10) from C_7H_{14}/D_2 mixtures contains 78% d_0, 19% d_1, and 3% d_2. This distribution suggests that "deuteration" occurs on a surface containing about 85% H* and 15% D* (predicted binomial distribution: 72% d_0, 24%

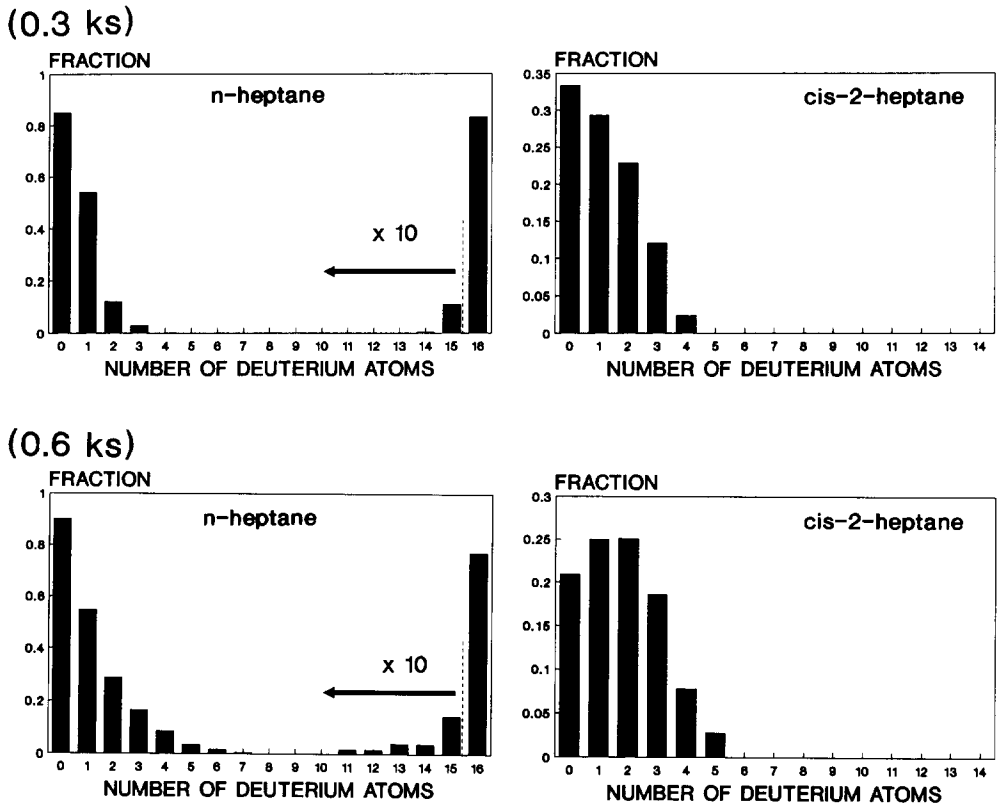

FIG. 11. Deuterium exchange with C_7D_{16}/C_7H_{14} mixtures. Deuterium distributions in *n*-heptane and *cis*-2-heptene (perdeuterated *n*-heptane, 3.5 kPa; 1-heptene, 1.3 kPa; deuterium, 20 kPa; 723 K).

d_1, 2% d_2). Such surfaces behave as if they were equilibrated with a gas-phase containing about 5.7 times more H_2 than D_2, rather than pure deuterium. Therefore, surface fugacities of hydrogen and deuterium are 114 and 20 kPa, respectively.

These deuteration studies confirm that hydrogen adsorption–desorption steps are not equilibrated during heptane and heptene dehydrogenation and dehydrocyclization reactions on Te/NaX. Hydrogen adatoms placed on surface sites by dehydrogenation steps are unable to equilibrate with corresponding gas-phase hydrogen species; their net removal from the surface as H_2 limits the overall rate of the catalytic sequence.

5. METHYLCYLOHEXANE DEHYDROGENATION ON Te/NaX

Cycloalkane dehydrogenation also involves the release of hydrogen adatoms onto surface sites, from which they must desorb for sites to "turnover." Methylcyclohexane dehydrogenates to intermediate methylcyclohexene and methylcyclohexadiene isomers and to stable toluene products on Te/NaX (Fig. 12a). The reaction proceeds without establishing 3-methyl-1-cyclohexene/methylcyclohexane equilibrium ratios (4.8×10^{-4}, steady state; 9.0×10^{-4} equilibrium) and without extensive exchange between methylcyclohexane and gas-phase D_2 (Fig. 13).

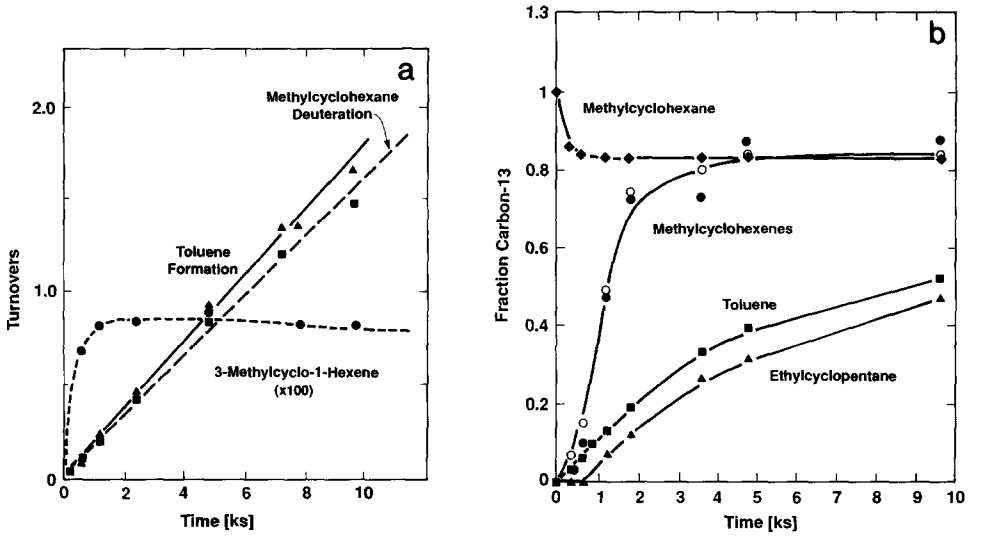

FIG. 12. Methylcyclohexane dehydrogenation on Te/NaX. (a) Turnovers for toluene and methylcyclohexene formation and methylcyclohexane deuteration (methylcyclohexane, 4.5 kPa; hydrogen (deuterium) 96 kPa; 673 K). (b) ^{13}C content in products of methylcyclohexane-1-^{13}C (79%) and 3-methylcyclo-1-hexene (21%) mixtures (4.5-kPa hydrocarbons; hydrogen, 96 kPa; 673 K).

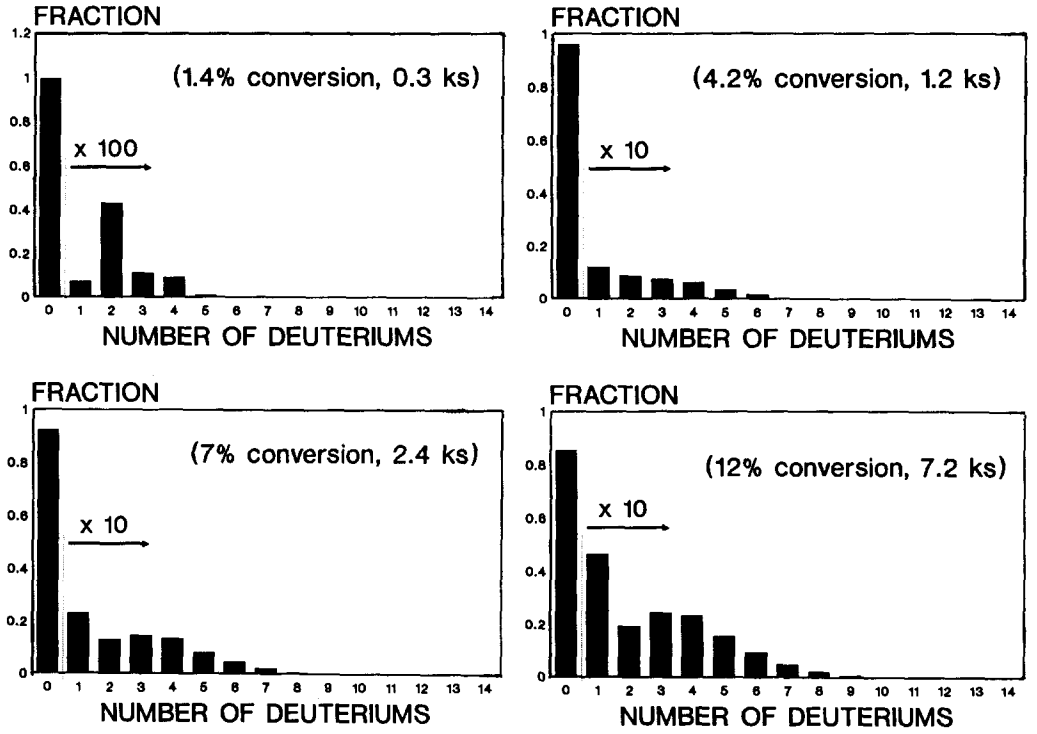

FIG. 13. Methylcyclohexane–deuterium exchange. Deuterium distributions in unreacted methylcyclohexane (methylcyclohexane, 4.5 kPa; deuterium 96 kPa; 673 K).

Competitive reactions of 3-methylcyclo-1-hexene (~20% mol) and [1-^{13}C]methylcyclohexane (~80% mol) show that initial toluene products are unlabeled (Fig. 12b); therefore, methylcyclohexenes are required intermediates in toluene formation:

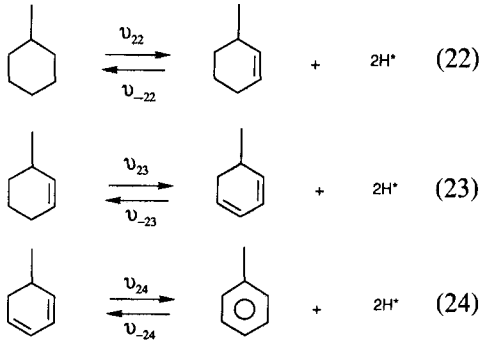

Isotopic ^{13}C equilibration between methylcyclohexane and methylcyclohexene occurs in about 2 ks (Fig. 12b), a time scale similar to that required for attaining steady-state methylcyclohexene concentrations (Fig. 12a). Measurements of unlabeled methylcyclohexane and unlabeled toluene turnovers allow us to obtain the ratio of methylcyclohexene hydrogenation (υ_{-22}) rate to that of its conversion to toluene products (υ_{23}). The initial value of this ratio ($\upsilon_{-22}/\upsilon_{23}$) is about 1.5 (Table 5).

The rate of deuterium incorporation into methylcyclohexane in the presence of D_2 is similar to the toluene formation rate (Fig. 12a). Their ratio ($\upsilon_{-22}/\upsilon_{23}$) is about 0.9 (Table 5). This value is lower than that obtained from ^{13}C isotopic tracer studies (1.5), suggesting that steady-state methylcyclohexane hydrogenation occurs on a surface containing about 60% D* and 40% H*. Thus, hydrogen adsorption–desorption is not equilibrated and recombinative desorption of hydrogen adatoms limits the rate of methylcyclohexane conversion to toluene. The surface hydrogen fugacity generated by dehydrogenation steps is about 65 kPa, while the corresponding deuterium surface fugacity equals its gas-phase pressure (96 kPa). Thus, the total surface hydrogen pressure is about 160 kPa (Table 5), in excellent agreement with the value calculated from deviations of steady-state cycloalkene/cycloalkane ratios from their equilibrium values (180 kPa).

TABLE 5

Methylcyclohexene Hydrogenation (υ_{-22}) and Conversion to Toluene (υ_{23}) Rates during Steady-State Methylcyclohexane Dehydrogenation (4.5-kPa Methylcyclohexane; 96-kPa H_2 or D_2; 673 K)

$(\upsilon_{-22}/\upsilon_{23})$ from ^{13}C exchange	1.5
$(\upsilon_{-22}/\upsilon_{23})$ from deuterium exchange	0.9
$(\upsilon_{-22}/\upsilon_{23})$ from methylcyclohexene to methylcylohexane steady-state ratio	0.9
$(H_2)_{ss}/(H_2)_g$	1.66
$(H_2)_{ss}$/(kPa)	160
% Deuterium in surface pool	60

6. PROPANE DEHYDROCYCLODIMERIZATION ON H-ZSM5 AND Ga/H-ZSM5

Propane reactions lead to products ranging from methane to C_{12} aromatics on H-ZSM5 (Table 6). The selectivity to C_{6+} aromatics is low and the hydrogen adatoms formed in dehydrogenation steps are removed from the surface predominantly by reaction with adsorbed hydrocarbon fragments, leading to methane and ethane; hy-

TABLE 6

Propane Turnover Rates and Product Distribution on H-ZSM5 and Ga/H-ZSM5 (773 K, 26.6-kPa C_3H_8, Balance He)

	H-ZSM5	2.0 wt% Ga/H-ZSM5
Propane conversion (%)	23.9	25.4
Turnover rate (s^{-1})	8.2×10^{-3}	2.3×10^{-2}
Carbon selectivity (%)		
CH_4	25.4	7.5
C_2H_4	18.7	12.6
C_2H_6	12.1	10.2
C_3H_6	16.6	17.9
C_4	14.9	7.3
C_5	1.1	0.46
Benzene	2.5	15.3
Toluene	5.1	18.3
Xylenes	3.0	9.5

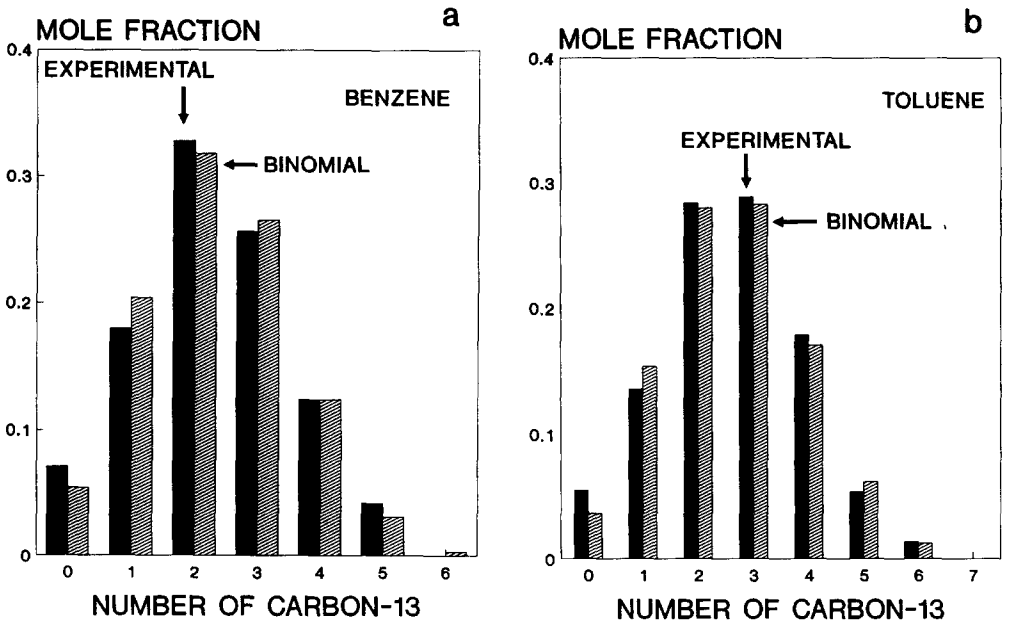

FIG. 14. Dehydrocyclodimerization of [2-^{13}C]propane on H-ZSM5. Isotopic composition of benzene and toluene products (773 K, 26.6 kPa C_3H_8, balance He, <15% propane converison).

drogen adatoms seldom desorb as dihydrogen, suggesting that recombinative desorption is slow on H-ZSM5.

Isotopic tracer studies of propene/[2-^{13}C]propane mixtures show that dehydrocyclodimerization occurs via alkene intermediates on H-ZSM5 and Ga/H-ZSM5. Alkenes enter oligomerization/cracking cycles that lead to the many skeletal isomerization events during one surface turnover; many C–C and C–H bonds are broken and reformed in one surface turnover. As a result, all products of [2-^{13}C]propane reactions on H-ZSM5 contain statistical numbers of ^{13}C atoms (Fig. 14). For example, benzene molecules with zero to five ^{13}C atoms are detected in the products of [2-^{13}C]propane reactions (Fig. 14a). Their relative isotopomer abundance obeys a binomial distribution, suggesting that the propane backbone is totally and randomly rearranged during reaction.

Every C–C and C–H bond in propane or propene reactants is broken and reformed several times during the formation of one product molecule. Thus, product molecules accurately sample the composition of the surface hydrogen pool; the deuterium content in the products of C_3H_8/D_2 reactants reflects the relative surface protium and deuterium fugacities and the extent to which hydrogen adsorption–desorption steps equilibrate during propane conversion. On H-ZSM5, deuterium contents are similar for all products (Fig. 15), suggesting that all products equilibrate with the same hydrogen surface fugacity. The deuterium content is low (2–4%); therefore, the surface hydrogen pool consists almost entirely of protium adatoms formed from reacting propane molecules rather than deuterium adatoms from gas-phase D_2. The deuterium surface fugacity equals its gas-phase value (6.6 kPa) because deuterium is not formed or consumed at significant rates during C_3H_8 conversion. The protium surface fugacity is 25–50 times greater than the deuterium pressure and leads to the measured 2–4% D in reaction products; the protium surface fugacity equals 165–330 kPa at reaction conditions.

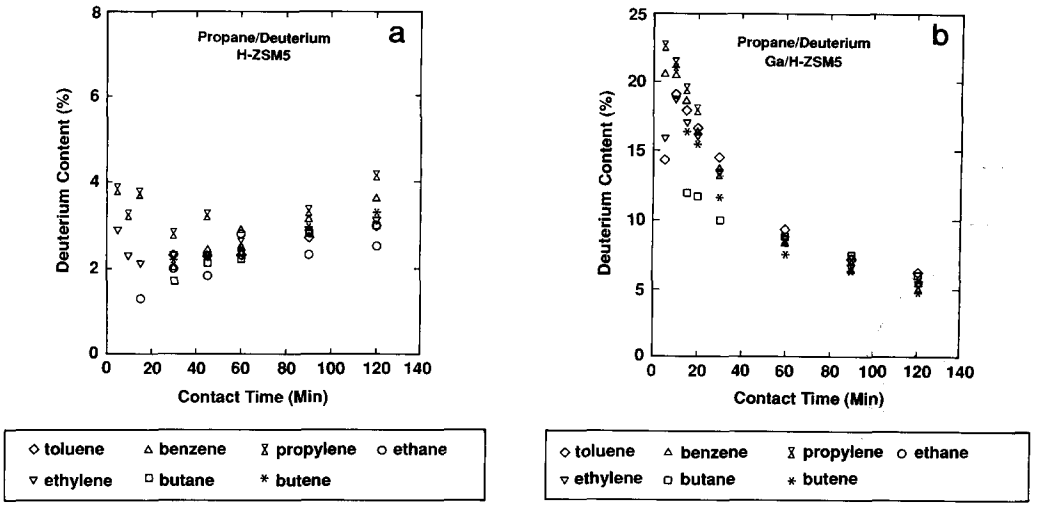

FIG. 15. Deuterium content in products of C_3H_8/D_2 reactions on H-ZSM5 and Ga/H-ZSM5 (773 K, 26.6 kPa C_3H_8, 6.6 kPa D_2, <15% propane conversion). (a) H-ZSM5. (b) 2.1 wt% Ga/H-ZSM5.

The presence of Ga ions (2.1 wt%) at exchange sites within zeolite channels increases propane conversion rate and C_{6+} aromatics selectivity and yield (Table 6). Ga selectively increases the rate of propane *and* propene dehydrogenation steps and leads to the appearance of dihydrogen as a gas-phase product. We propose that Ga ions exchanged onto cationic sites in ZSM5 act as "portholes" (*37*) for the recombinative desorption of hydrogen adatoms; in this manner, Ga ions lower hydrogen surface fugacities at catalytic sites on H-ZSM5. In the presence of Ga, cracking reactions are no longer required for removing all hydrogen adatoms formed in dehydrogenation steps. Aromatics can be formed without concurrent cracking events and the C_{6+} aromatics selectivity increases (43.1% vs 10.6%, Table 6).

Ga ions increase the deuterium content in propane reaction products (Fig. 15); all products initially contain about 25% D, a value much higher than that on H-ZSM5 (2–4% D). The deuterium content in the products decreases as contact time increases (Fig. 15) because gas-phase D_2 is diluted by the H_2 product formed in C_3H_8 reactions. Products are formed on catalytic sites that contain about 25% D-atoms (from gas-phase D_2) and 75% H-atoms (from reacting propane molecules). Again, the surface deuterium fugacity equals its gas-phase value (6.6 kPa) and protium virtual pressures are about three times greater (20 kPa). Thus, the total hydrogen surface fugacity is much lower on Ga/H-ZSM5 (26.6 kPa) than on H-ZSM5 (165–330 kPa); however, gas-phase and surface hydrogen pools remain nonequilibrated and modest protium surface fugacities remain during propane conversion on H-ZSM5 even in the presence of Ga ions.

Recombinative desorption of hydrogen adatoms limits propane conversion rates and aromatics selectivity on H-ZSM5. Dehydrogenation rates and steady-state concentrations of unsaturated intermediates are decreased by high surface hydrogen fugacities that also lead to hydrocracking as the predominant hydrogen removal pathway. We propose that Ga ions partially relieve these hydrogen overpressures by catalyzing the recombinative desorption of H-adatoms

during propane conversion. This porthole effect probably accounts also for similar effects of Pt and Zn on the rate and selectivity of propane conversion on H-ZSM5 (*18–25, 38, 39*). The earliest evidence for hydrogen desorption portholes was reported by H. S. Taylor in 1961 (*37*): Pt surfaces catalyzed the desorption of hydrogen adatoms during the decomposition of GeH_2 to Ge metal. Undoubtedly, hydrogen desorption portholes also play a crucial role in controlling hydrogen transfer reactions (*35*) that occur in catalytic cracking processes.

The enhancing effect of Pt, Ga, and Zn species on propane dehydrocyclodimerization rates and aromatics selectivity on HZSM-5 (*21–25, 38, 39*) is consistent with reaction rates limited by hydrogen desorption. Metals and low-valent metal ions such as $Ga^{+\delta}$ enhance dehydrogenation rates of alkanes, alkenes, and cycloalkanes on zeolitic and nonzeolitic metal oxides (*38–40*) and on active carbon (*41*) by increasing the rate of alkane dehydrogenation (*39*) and of hydrogen removal as H_2 (*38, 40, 41*) during alkane reactions. We suggest that an acid functionality (such as HZSM-5 or SiO_2/Al_2O_3) can carry out stoichiometric paraffin dehydrogenation and olefin dimerization and cyclization reactions. Yet, sites cannot turnover without hydrogen desorption sites (e.g., Ni, Cu, $Zn^{+\delta}$ (*38*), $Ga^{+\delta}$ (*40*), noble metals (*41*), metal chromites, or mixtures thereof) that provide an efficient porthole for the removal of the hydrogen adatoms formed in dehydrogenation steps.

Our work shows conclusively that $Ga^{+\delta}$ ions enhance the interaction between gas-phase and surface hydrogen pools by increasing the rate of hydrogen adsorption–desorption. However, complete equilibration does not occur even at high Ga loadings (2.0 wt%) and hydrogen removal remains one of the rate-limiting steps even on Ga/H-ZSM5 catalysts.

Recombinative desorption of hydrogen adatoms from metal oxides and nonmetals occurs by heterolytic recombination of H^+ and H^- species. Most previous studies have addressed the reverse step: the heterolytic dissociation of H_2 on such surfaces (*42, 43*). Heterolytic dissociation of H_2 leads to the formation of protons stabilized by the metal cation and hydride species associated with the oxygen anions (*42*):

$$H_2(g) + M^{+\delta}O_s^{-2} \rightleftarrows H^- M^{+\delta} + H^+ - O_s^{-2}. \quad (25)$$

A subsequent redox process

$$H^- M^{+\delta} + M^{+\delta}O_s^{-2} \rightleftarrows 2M^{+(\delta-1)}O_s^{-2}H^+ \quad (26)$$

can lead to the formation of additional protons and to the partial reduction of a neighboring metal cation (*43*). This latter process occurs only on oxides of metals with multiple valence states.

We propose that recombinative desorption of hydrogen adatoms occurs on Te/NaX and Ga/H-ZSM5 by the reverse of Eq. (25),

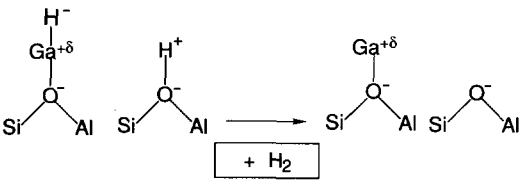

(27)

perhaps with a slight decrease in the metal oxidation state (Eq. (27)) in order to decrease the net negative charge of the hydride ion. Thus, Ga and Te ions act as Lewis acids that stabilize the negative charge in H^- species. In the absence of such low-valent ions, zeolites momentarily stabilize hydride ions by adsorption on Al atom sites that lack neighboring protonated O^- sites. These unstable hydride species are likely to recombine with the hydrocarbon that formed them or with neighboring hydrocarbon fragments

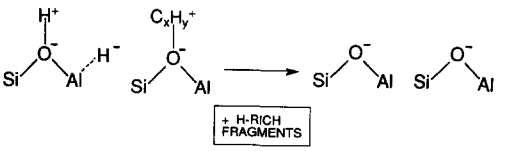

(28)

in order to form hydrogen-rich cracking products; they are unlikely to react with protons associated with distant Brønsted sites unperturbed by hydride ions on associated Al ions.

7. CONCLUSIONS

We have provided experimental evidence for the rate-determining role of hydrogen desorption steps and for the presence of hydrogen surface fugacities that exceed gas-phase hydrogen pressures during *n*-heptane dehydrocyclization and methylcyclohexane dehydrogenation on Te/NaX and during propane dehydrocyclodimerization on H-ZSM5 and Ga/H-ZSM5. Hydrogen desorption limits the rate of the intermediate dehydrogenation steps required in these alkane reactions. High surface hydrogen fugacities decrease the concentration of unsaturated intermediates by limiting them to values in equilibrium with surface hydrogen fugacities that significantly exceed gas-phase dihydrogen pressures.

Hydrogen desorption rates can be increased by metal ions such as $Te^{+\delta}$, $Ga^{+\delta}$, and others; they act as catalysts for the rate-determining hydrogen desorption steps. Hydrogen removal rates can also be increased by surface reactions that attach it to a surface hydrocarbon fragment (hydrocracking) or to an unsaturated adsorbed molecule (hydrogenation). Thus, alkanes can be used as effective hydrogen sources for desired hydrogenation and hydrocracking reactions; in this manner, we can benefit from high hydrogen surface fugacities that would otherwise limit the rate of alkane dehydrogenation reactions.

APPENDIX: NOMENCLATURE

f fugacity

$\vec{\nu}_i$ turnover rate in forward direction for ith step

$\overleftarrow{\nu}_i$ turnover rate in reverse direction for ith step

$\vec{\nu},\overleftarrow{\nu}$ overall turnover rates in forward and reverse for a catalytic sequence at steady state

$A_i(A_i^0)$ (standard) reaction affinity of ith step ($= -\Delta G_i$)

ν_i stoichiometric number of ith elementary step in catalytic sequence

R_{ss} steady-state heptene/*n*-heptane ratio

R_{eq} equilibrium heptene/*n*-heptane ratio

$\overline{\mathbf{K}}_{(i)}$ equilibrium constant for overall reaction (ith elementary step)

χ ratio of steady-state to equilibrium heptene to heptane ratio

$\vec{k}_i,\overleftarrow{k}_i$ rate constants for ith step in forward and reverse reactions

k_a adsorption rate constant

k_d desorption rate constant

Subscripts/Superscripts

i elementary step or reaction

0 standard value of affinity

g gas phase

ss steady state

eq equilibrium

REFERENCES

1. Anderson, J. R., *in* "Advances in Catalysis" (D. D. Eley, H. Pines, and P. B. Weisz, Eds.), Vol. 23, p. 1. Academic Press, New York, 1973.
2. Gault, F. G., *in* "Advances in Catalysis" (D. D. Eley, H. Pines, and P. B. Weisz, Eds.), Vol. 30, p. 1. Academic Press, New York, 1981.
3. Sinfelt, J. H., *in* "Advances in Catalysis" (D. D. Eley, H. Pines, and P. B. Weisz, Eds.), Vol. 23, p. 91. Academic Press, New York, 1973.
4. (a) Iglesia, E., Baumgartner, J. E., Price, G. L., Rose, K. D., and Robbins, J. L., *J. Catal.* **125,** 95, (1990); (b) Iglesia, E., Baumgartner, J. E., and Price, G. L., *in* "11th North American Catalysis Society Meeting, Dearborn, Michigan, 1989"; (c) Iglesia, E., Baumgartner, J. E., and Price, G. L., *in* "AIChE National Meeting, Philadelphia, Pennsylvania, 1989."
5. Kemball, C., *Discuss. Faraday Soc.* **41,** 190 (1966).
6. Brieger, G., and Nestrick, T. J., *Chem. Rev.* **74,** 567 (1974); Kolomnikov, I. S., Kukolev, V. P., and Vol'pin, M. E., *Russ. Chem. Rev.* **43,** 399 (1974).
7. Corson, B. B., and Ipatieff, V. N., *J. Am. Chem. Soc.* **61,** 1056 (1939).
8. Boudart, M., *Catal. Lett.* **3,** 111 (1989).
9. Miale, J. N., and Weisz, P. B., *J. Catal.* **20,** 288 (1971).

10. Lang, W. H., Mikovsky, R. J., and Silvestri, A. J., *J. Catal.* **20,** 293 (1971).
11. Mikovsky, R. J., Silvestri, A. J., Dempsey, E., and Olson, D. H., *J. Catal.* **22,** 371 (1971).
12. Olson, D. H., Mikovsky, R. J., Shipman, G. F., and Dempsey, E., *J. Catal.* **24,** 161 (1972).
13. Silvestri, A. J., and Smith, R. L., *J. Catal.* **29,** 316 (1973).
14. Price, G. L., Ismagilov, Z. R., and Hightower, J. W., *in* "Proceedings, 7th International Congress on Catalysis, Tokyo, 1980"., (T. Seiyama and K. Tanabe, Eds.), Part A, p. 708. Elsevier, Amsterdam/New York, 1981.
15. Price, G. L., Ismagilov, Z. R., and Hightower, J. W., *J. Catal.* **73,** 361 (1982).
16. Price, G. L., Ismagilov, Z. R., and Hightower, J. W., *J. Catal.* **81,** 369 (1983).
17. Price, G. L., and Egedy, C., *J.Catal.* **84,** 461 (1983).
18. Csicsery, S. M., *J. Catal.* **17,** 207 (1970).
19. Csicsery, S. M., *J. Catal.* **17,** 216 (1970).
20. Csicsery, S. M., *Ind. Eng. Chem. Process Des. Dev.* **18,** 191 (1979).
21. Bragin, O. V., Shapiro, E. S., Preobrazhensky, A. V., Isaev, S. A., Vasina, T. V., Dyusenvina, B. B., Antoshin, G. V., and Minachev, Kh. M., *Appl. Catal.* **27,** 219 (1986).
22 Gregory, R., and Kolombos, A. J., United States Patent 4,056,575 (1977).
23. Bulford, S. N., and Davies, E. E., United States Patent 4,157,356 (1979).
24. Kitagawa, H., Sendoda, Y., and Ono, Y., *J. Catal.* **101,** 12 (1986).
25. Mowry, J. R., Anderson, R. F., and Johnson, J. A., *Oil Gas J.* **83,** 128 (1985).
26. Temkin, M. I., and Pyzhev, V., *Zhur. Fiz. Khim.* **13,** 851 (1939).
27. Temkin, M. I., and Pyzhev, V., *Acta Physicochim.* **12,** 327 (1940).
28. Shinda, H., Egawa, C., Onishi, T., and Tamaru, K., *J. Chem. Soc. Faraday Trans.* 1 **76,** 280 (1980).
29. Boudart, M., Egawa, C., Oyama, S. T., and Tamaru, K., *J. Chim. Phys.* **78,** 987 (1981).
30. Boudart, M., *J. Phys. Chem.* **87,** 2786 (1983).
31. Boudart, M., *Ind. Eng. Chem. Fundam.* **25,** 70 (1986).
32. Yashima, T., Sasaki, T., Takahashi, K., Watanabe, S., and Namba, S. *Sekiyu Gakkaishi* **31,** 154 (1988).
33. Price, G. L., and Iglesia, E., *Ind. Eng. Chem.* **28,** 839 (1989).
34. Stull, D. R., Westrum, E. F., Jr., and Sinke, G. C., "The Chemical Thermodynamics of Organic Compounds." Wiley, New York, 1969.
35. Abbott, J., and Head, J. D., *J. Catal.* **125,** 187 (1990).
36. Iglesia, E., unpublished results.
37. Taylor, H. S., *Ann. Rev. Phys. Chem.* **12,** 127 (1961); *in* "Proceedings, 2nd International Congress on Catalysis, Paris, 1960," p. 159. Technip, Paris, 1961.
38. Mole, T., Anderson, J. R., and Creer, G., *Appl. Catal.* **17,** 141 (1985).
39. Meriaudaeu, P., and Nacchache, C., *J. Mol. Catal.* **59,** L31, 1990.
40. Yao, J., le van Mao, R., and Dufresne, L., *Appl. Catal.* **65,** 175 (1990).
41. Fujimoto, K., and Toyoshi, S., *in* "Proceedings, 7th International Congress on Catalysis, Tokyo, 1980" (T. Seiyama and K. Tanabe, Eds.), Part A, p. 235. Elsevier, Amsterdam/New York, 1981.
42. Dent, A. L., and Kokes, R. J., *J. Phys. Chem.* **73,** 3781 (1969).
43. Burwell, R. L., Haller, G. L., Taylor, K. C., and Read, J. F., *in* "Advances in Catalysis" (D. D. Eley, H. Pines, and P. B. Weisz, Eds.), Vol. 20, p. 1. Academic Press, New York, 1969.